

The Warped Plane of the Classical Kuiper Belt

Eugene Chiang¹ and Hyomin Choi²

echiang@astro.berkeley.edu, hyomin@berkeley.edu

ABSTRACT

By numerically integrating the orbits of the giant planets and of test particles over a period of four billion years, we follow the evolution of the location of the midplane of the Kuiper belt. The Classical Kuiper belt conforms to a warped sheet that precesses with a 1.9 Myr period. The present-day location of the Kuiper belt plane can be computed using linear secular perturbation theory: the local normal to the plane is given by the theory's forced inclination vector, which is specific to every semi-major axis. The Kuiper belt plane does not coincide with the invariable plane, but deviates from it by up to a few degrees in stable zones. For example, at a semimajor axis of 38 AU, the local Kuiper belt plane has an inclination of 1.9 degrees and a longitude of ascending node of 149.9 degrees when referred to the mean ecliptic and equinox of J2000. At a semimajor axis of 43 AU, the local plane has an inclination of 1.9 degrees and a nodal longitude of 78.3 degrees. Only at infinite semimajor axis does the Kuiper belt plane merge with the invariable plane, whose inclination is 1.6 degrees and nodal longitude is 107.7 degrees. A Classical Kuiper belt object keeps its inclination relative to the Kuiper belt plane nearly constant, even while the latter plane departs from the trajectory predicted by linear theory. The constancy of relative inclination reflects the undamped amplitude of free oscillation; that is, the homogeneous solution to the forced harmonic oscillator equation retains constant amplitude, even while the inhomogeneous solution cannot be written down accurately because the planetary forcing terms are chaotic. Current observations of Classical Kuiper belt objects are consistent with the plane being warped by the giant planets alone, but the sample size will need to increase by a few times before confirmation exceeds 3σ in confidence. In principle, differences between the theoretically expected plane and the observed plane could be used to infer as yet unseen masses orbiting the Sun, but carrying out such a program would be challenging.

¹Center for Integrative Planetary Sciences, Department of Astronomy, University of California at Berkeley, Berkeley, CA 94720, USA

²Department of Mathematics, University of California at Berkeley, Berkeley, CA 94720, USA

Subject headings: comets: general — Kuiper belt — solar system: general — celestial mechanics

1. INTRODUCTION

If we could map, at fixed time, the instantaneous locations in three-dimensional space of all Kuiper belt objects (KBOs), on what two-dimensional surface would the density of KBOs be greatest? We call this surface the plane of the Kuiper belt (KBP), though by “plane” we do not mean to imply that the KBP is flat (we shall find that it is not). The KBP depends on the mass distribution of the solar system—principally, the orbits and masses of the giant planets. There are as many different KBPs as there are dynamical classes of KBO, since each class of object feels a distinct time-averaged force. Here we study the KBP defined by Classical KBOs: objects whose fairly circular, low inclination orbits are not in any strong mean-motion resonance with Neptune (see Elliot et al. 2005 for a classification scheme).

In principle, theoretical determination of the KBP would help observers to discover new KBOs. Conversely, by measuring differences between the theoretical KBP and the actual KBP, we might hope to infer the presence of solar system bodies as yet undetected (“Planet X”; see Gaudi & Bloom 2005 for a summary of current limits).

There is disagreement regarding the location of the KBP. Brown & Pan (2004) analyzed the instantaneous proper motion vectors of hundreds of KBOs irrespective of dynamical class and concluded, with greater than 3σ confidence, that the KBP did not coincide with the invariable plane (IP, the plane perpendicular to the total angular momentum vector of the solar system). They argued that the observed KBP was consistent instead with the forced plane given by linear secular perturbation theory. We will refer to this plane as the BvWP, after Brouwer & van Woerkom (1950), who developed a linear secular theory for the motions of all eight of the major planets. Their theory, in turn, has its origin in the Laplace-Lagrange equations (see, e.g., Murray & Dermott 1999). The BvWP is a warped and time-variable surface whose properties we review in §2.

By contrast, Elliot et al. (2005) found that the plane determined by Classical KBOs that were observed over multiple epochs was more consistent with the IP ($\lesssim 1\sigma$ difference) than with the BvWP ($\lesssim 2\text{--}3\sigma$ difference). They listed some arguments, none conclusive, for why the IP might be preferred over the BvWP. The low order of the BvW theory, and its inability to account for time variations in semi-major axes, are causes for concern.

We seek to resolve this disagreement using numerical orbit integrations. In §2, we review the linear theory and how it equates the KBP with the BvWP. In §3, numerical integrations

lasting the age of the solar system are used to reveal the theoretical location of the KBP. In §4, we compare theory against current observations of the KBP. A summary is given in §5, including a brief comment on the prospects for detecting an unseen, outer solar system planet using the KBP.

2. LINEAR SECULAR THEORY

We study the secular evolution of Classical KBOs by solving the Laplace-Lagrange equations of motion, which neglect all terms higher than second order in orbital eccentricity (e) and orbital inclination (i). The solution is detailed in the textbook by Murray & Dermott (1999); we provide a summary here.

We start by describing the motions of the planets. Define an inclination vector $\mathbf{i} \equiv (q, p) \equiv (i \cos \Omega, i \sin \Omega)$, where i and Ω equal the inclination and longitude of ascending node. Lagrange’s equations governing the inclination vector for the j th planet are

$$\dot{q}_j = -\frac{1}{n_j a_j^2} \frac{\partial R_j}{\partial p_j} \quad (1)$$

$$\dot{p}_j = \frac{1}{n_j a_j^2} \frac{\partial R_j}{\partial q_j}, \quad (2)$$

where n_j , a_j , and R_j are, respectively, the mean motion, semi-major axis, and disturbing function. We consider only the four giant planets so that $j = 1, 2, 3, 4$ represents Jupiter, Saturn, Uranus, and Neptune, respectively. The disturbing function, keeping only the leading terms relevant to the inclination evolution of the j th planet, reads

$$R_j = -\frac{n_j^2 a_j^2}{8} \sum_{k=1, \neq j}^4 \frac{m_k}{M_\odot + m_j} \alpha_{jk} \bar{\alpha}_{jk} b_{3/2}^{(1)}(\alpha_{jk}) [q_j^2 + p_j^2 - 2(q_j q_k + p_j p_k)],$$

where $b_{3/2}^{(1)}(\alpha_{jk})$ is a Laplace coefficient,¹ m_j is the mass of the j th planet,

$$\alpha_{jk} = \begin{cases} a_k/a_j & \text{if } a_j > a_k \\ a_j/a_k & \text{if } a_j < a_k \end{cases}$$

¹ If we declare $\alpha_{jk} = \bar{\alpha}_{jk} = a_j/a_k$ and allow the Laplace coefficient to take $\alpha_{jk} > 1$ as an argument, then separating the case $a_j < a_k$ from $a_j > a_k$ is not necessary. We stick here with the textbook convention, however.

and

$$\bar{\alpha}_{jk} = \begin{cases} 1 & \text{if } a_j > a_k \\ a_j/a_k & \text{if } a_j < a_k. \end{cases}$$

Eqns. (1)–(2) yield two coupled systems of first-order differential equations: $(\dot{p}_1, \dot{p}_2, \dot{p}_3, \dot{p}_4)^T = A(q_1, q_2, q_3, q_4)^T$ and $(\dot{q}_1, \dot{q}_2, \dot{q}_3, \dot{q}_4)^T = -A(p_1, p_2, p_3, p_4)^T$, where A is a 4×4 matrix of constant coefficients depending on the masses and semi-major axes of the planets. These equations describe coupled harmonic oscillators; their solution is

$$q_j = \sum_{k=1}^4 I_{jk} \cos(f_k t + \gamma_k) \quad (3)$$

$$p_j = \sum_{k=1}^4 I_{jk} \sin(f_k t + \gamma_k), \quad (4)$$

where the frequencies f_k are the eigenvalues of A . The elements I_{jk} of the eigenvectors of A , and the phases γ_k , are fitted to the initial inclinations and ascending nodes of the planets. We take initial conditions and planetary data from the NASA JPL Horizons database for JD = 2451544.5 (Jan 1 2000; $t = 0$ in equations (3) and (4)). Table 1 lists the resultant values for f_k , I_{jk} , and γ_k . We refer to this solution as the BvW solution, even though Brouwer and van Woerkom (1950) included all eight planets.

We now turn to our main concern, the motion of a KBO of negligible mass with semi-major axis $a > a_j$. Its disturbing function is

$$R = -\frac{n^2 a^2}{8} \sum_{j=1}^4 \frac{m_j}{M_\odot} \frac{a_j}{a} b_{3/2}^{(1)}(a_j/a) [q^2 + p^2 - 2(qq_j + pp_j)],$$

where unsubscripted variables refer to the KBO. Because all masses and semi-major axes are fixed for this secular problem, Lagrange's equations of motion are of the form

$$\dot{q} = -\frac{1}{na^2} \frac{\partial R}{\partial p} = -c_0 p + \sum_{j=1}^4 c_j p_j$$

$$\dot{p} = \frac{1}{na^2} \frac{\partial R}{\partial q} = +c_0 q - \sum_{j=1}^4 c_j q_j,$$

where the c 's are constants. Substituting each equation into the time derivative of the other, we find

$$\ddot{q} = -c_0^2 q + \sum_{j=1}^4 c_j [c_0 q_j(t) + \dot{p}_j(t)] \quad (5)$$

$$\ddot{p} = -c_0^2 p + \sum_{j=1}^4 c_j [c_0 p_j(t) - \dot{q}_j(t)]. \quad (6)$$

Eqns. (5)–(6) describe harmonic oscillators of natural frequency c_0 , forced by the planetary terms in the sums. The motion is composed of a forced oscillation and a free oscillation:

$$q = q_{\text{forced}} + q_{\text{free}} = q_{\text{forced}} + i_{\text{free}} \cos(ft + \gamma) \quad (7)$$

$$p = p_{\text{forced}} + p_{\text{free}} = p_{\text{forced}} + i_{\text{free}} \sin(ft + \gamma), \quad (8)$$

where i_{free} and γ are constants determined by initial conditions, and the free precession frequency

$$f = c_0 = \sum_{j=1}^4 c_j = -\frac{n}{4} \sum_{j=1}^4 \frac{m_j}{M_\odot} \frac{a_j}{a} b_{3/2}^{(1)}(a_j/a).$$

The functions q_{forced} and p_{forced} depend only on planetary parameters and the KBO semi-major axis a :

$$q_{\text{forced}} = -\sum_{k=1}^4 \frac{\mu_k}{f - f_k} \cos(f_k t + \gamma_k) \quad (9)$$

$$p_{\text{forced}} = -\sum_{k=1}^4 \frac{\mu_k}{f - f_k} \sin(f_k t + \gamma_k) \quad (10)$$

where

$$\mu_k = -\sum_{j=1}^4 c_j I_{jk} = \frac{n}{4} \sum_{j=1}^4 I_{jk} \frac{m_j}{M_\odot} \frac{a_j}{a} b_{3/2}^{(1)}(a_j/a).$$

The inclination vector \mathbf{i} of a KBO is the vector sum of a forced inclination vector $\mathbf{i}_{\text{forced}} \equiv (q_{\text{forced}}, p_{\text{forced}})$ and a free inclination vector $\mathbf{i}_{\text{free}} \equiv (q_{\text{free}}, p_{\text{free}})$. Throughout this paper, we refer to a forced inclination $i_{\text{forced}} \equiv (q_{\text{forced}}^2 + p_{\text{forced}}^2)^{1/2}$, a forced node $\Omega_{\text{forced}} \equiv \arctan(p_{\text{forced}}/q_{\text{forced}})$, a free inclination $i_{\text{free}} \equiv (q_{\text{free}}^2 + p_{\text{free}}^2)^{1/2}$, and a free node $\Omega_{\text{free}} \equiv \arctan(p_{\text{free}}/q_{\text{free}})$. Thus free and forced inclinations refer to magnitudes (not vectors). The free inclination is constant; it is the undamped amplitude of the free oscillation.

Figure 1 shows the evolution of $\mathbf{i}_{\text{forced}}$ at various semi-major axes in the Kuiper belt. The open diamonds, located at the endpoints of $\mathbf{i}_{\text{forced}}$, mark what we call the forced poles. At fixed time, the forced poles all lie along a line intersecting the invariable pole, denoted \mathbf{I} . To the extent that the $k = 4$ mode, driven mainly by Neptune, dominates, the forced poles rotate clockwise (regress) about the invariable pole at a single frequency (f_4), maintaining constant distance to \mathbf{I} . Note that the forced poles at $a > 40.5\text{AU}$ lie diametrically opposite to those at $a < 40.5\text{AU}$, and that as a approaches 40.5AU from either above or below, the

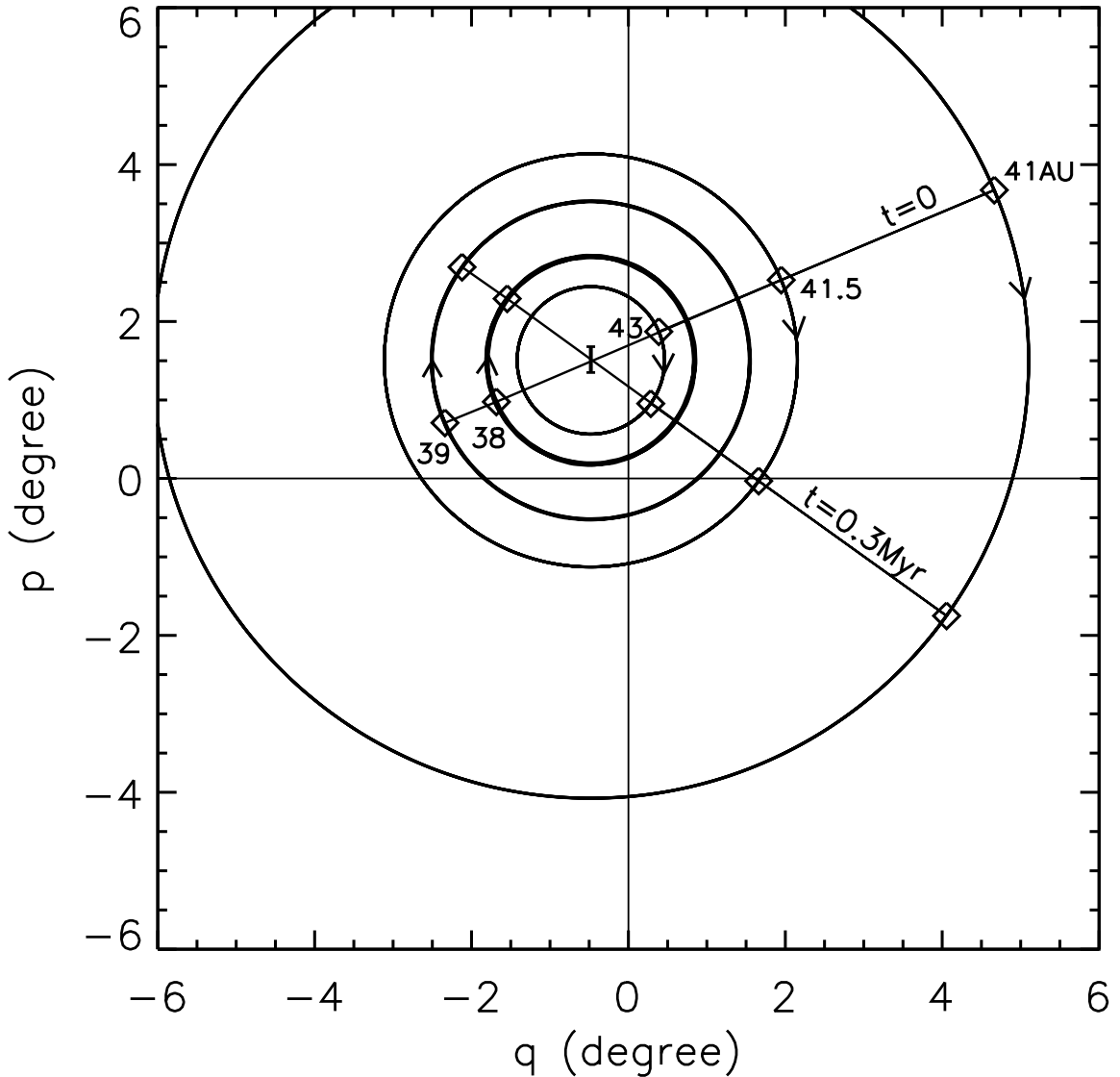


Fig. 1.— Locations of forced poles (open diamonds) at various semi-major axes, at $t = 0$ (JD = 2451544.5) and $t = 0.3$ Myr. Coordinates are referenced to the ecliptic and mean equinox of J2000 (the origin marks the location of the J2000 ecliptic pole). The invariable pole is marked by “I.” Note how the forced poles at $a > 40.5$ AU lie diametrically opposite to those at $a < 40.5$ AU, reflecting forcing by the ν_{18} resonance at $a = 40.5$ AU. As a approaches 40.5 AU, the forced pole diverges from the invariable pole. As a increases beyond 40.5 AU, the forced pole approaches the invariable pole. We show in this paper that the forced poles point normal to the Kuiper belt plane.

separation between the forced pole and \mathbf{I} increases. These latter two properties reflect the ν_{18} secular resonance at $a = 40.5\text{AU}$, where the denominators $f - f_4$ of equations (9)–(10) vanish: the forced response becomes infinite in magnitude at resonance, and changes phase by 180° across resonance (the sign of $f - f_4$ switches across $a = 40.5\text{AU}$).

Figure 2 illustrates how free nodes Ω_{free} phase mix and how such phase mixing helps determine the KBP within the BvW theory. At $t = 0$, one hundred KBOs having semi-major axes within 0.5 AU of 43 AU are set down with orbit normals approximately aligned about an arbitrary direction (the orbit poles are actually distributed in a small box in p - q space). Over tens of Myrs, the orbit poles of the particles drift away from one another: the small dispersion in semi-major axis produces a small dispersion in the free precession frequency f (the rate at which the free inclination vector rotates about the forced pole).² While the free nodes distribute themselves over all phases, the free inclinations i_{free} remain fixed. Thus, at late times, the collection of free inclination vectors \mathbf{i}_{free} are distributed axisymmetrically about the mean forced pole at $a \approx 43$ AU. The axisymmetry arises practically independently of how the particles’ orbit normals are initially distributed; the only requirements are that many particles share the same i_{free} (so that such particles, when phase mixed, trace a full circle) and that there exists a small but non-zero dispersion in semi-major axis (so that there exists a non-zero spread in free precession frequencies, enabling phase mixing). Note in Figure 2 how the invariable pole does not coincide with the center of the circular distribution.

We conclude that according to the BvW theory, the mean orbit normal of a phase-mixed group of particles having approximately the same semi-major axis is given by the forced pole corresponding to that semi-major axis. That local forced pole varies with time (Figure 1), but the particles always encircle it (Figure 2). The KBP is warped because the forced pole changes direction with KBO semi-major axis (Figure 1).

Note finally that the ability of test particles to keep their free inclinations constant relative to a time-variable forced pole should not be confused with adiabatic invariance. Generally the frequencies f and f_k are not cleanly separated. The constant i_{free} simply reflects the undamped amplitude of free oscillation, and is set by initial conditions. In the next section, we use numerical simulations to test the constancy of free inclination.

²In the linear theory, precession frequencies f and f_k do not depend on eccentricity or inclination, but in higher order theories they do.

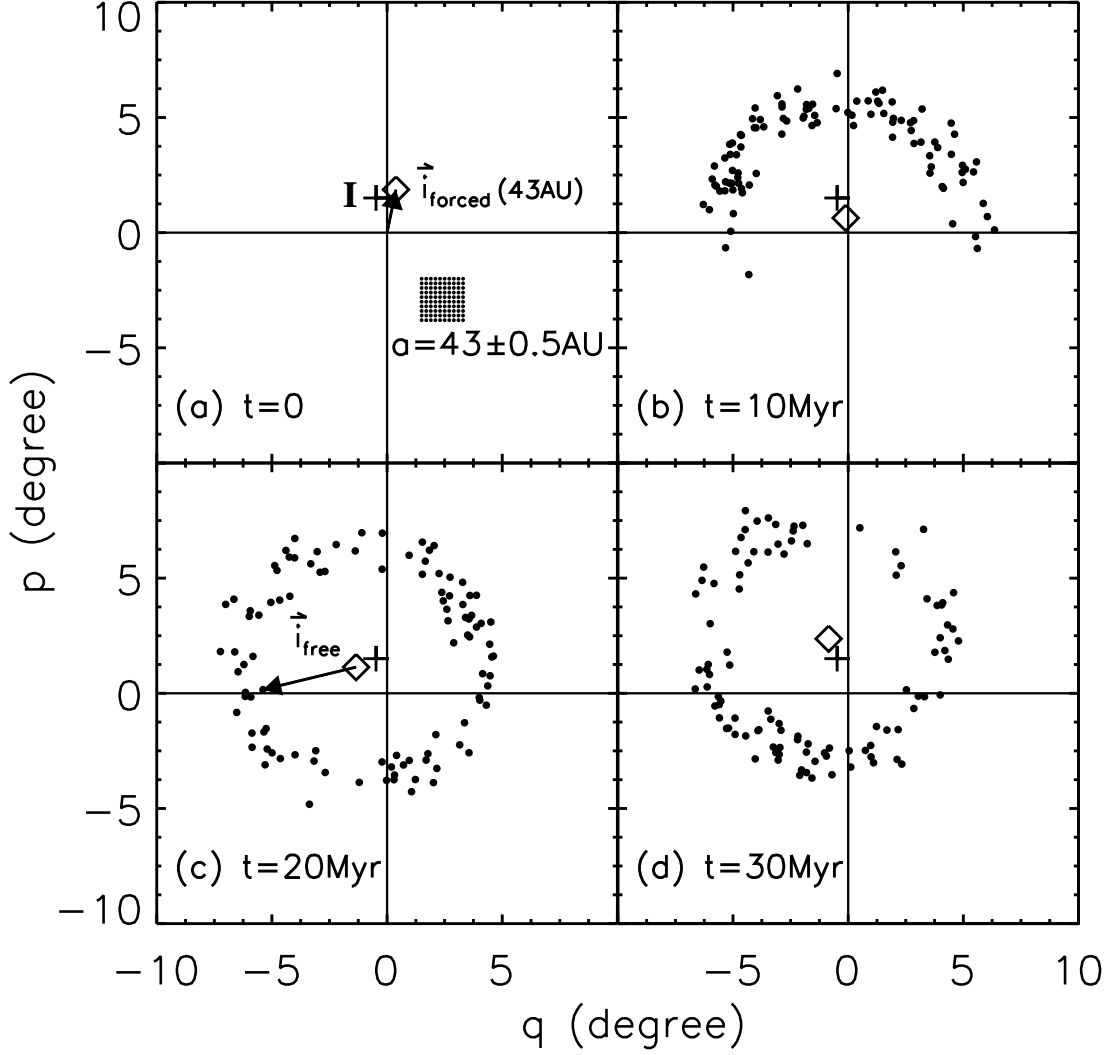


Fig. 2.— Phase mixing and axisymmetry of KBOs about the forced pole. In panel (a), the orbit poles of 100 test particles (solid circles), having semi-major axes randomly distributed between 42.5 and 43.5 AU, are distributed on a grid in p - q space. The forced pole at $a = 43$ AU (open diamond) and the invariable pole (“+”) are indicated. As time elapses from panels (b) through (d), the poles of the test particles precess about the forced pole, which itself precesses about the invariable pole. Precession rates differ from one particle to the next according to their semi-major axes, while the distance from each pole to the forced pole—the free inclination (see panel c)—remains constant. Consequently, after a few tens of Myrs, orbit poles tend to phase mix into an annulus centered on the forced pole (not the invariable pole). The evolution shown here was computed using the analytic BvW solution, not the numerical integration.

3. NUMERICAL INTEGRATIONS

3.1. Initial Conditions

We calculate the evolution of the KBP at three semi-major axes: $a = 38, 43,$ and 44 AU. These are chosen to lie away from strong mean-motion resonances (e.g., the 3:2 resonance resides at 39.5 AU) and outside the $a = 40\text{--}42$ AU region of instability carved by the ν_{18}, ν_{17} and ν_8 secular resonances (see, e.g., Chiang et al. 2007). At each a we lay down $N_i \times N_\Omega$ test particles whose initial free inclination vectors are distributed axisymmetrically about the local forced pole. That is, each particle’s initial $p = p_{\text{forced}}(a) + p_{\text{free}}$ and initial $q = q_{\text{forced}}(a) + q_{\text{free}}$, where $i_{\text{free}} = (p_{\text{free}}^2 + q_{\text{free}}^2)^{1/2}$ takes 1 of $N_i = 4$ values (0.01, 0.03, 0.1, 0.3 rad) and $\Omega_{\text{free}} = \arctan(p_{\text{free}}/q_{\text{free}})$ takes 1 of $N_\Omega = 20$ values distributed uniformly between 0 and 2π . This set-up permits us to directly test the BvW theory, which predicts that all N_Ω particles corresponding to a given a and given initial i_{free} should keep the same i_{free} for all time: a circle of points in p - q space should continue to trace the same-sized circle. Coordinates p_{forced} and q_{forced} for the initial forced poles are computed using the BvW solution of §2, for $t = 0$.

Initial osculating eccentricities are zero and initial mean anomalies are chosen randomly between 0 and 2π . The four giant planets are included in the integration, with initial conditions taken from the JPL Horizons database for JD = 2451544.5 ($t = 0$ in the BvW theory). The integration is performed with the `swift_rmvs3` code, written by Levison & Duncan (1994) and based on the algorithm developed by Wisdom & Holman (1991). The duration of the integration is 4 Gyr and the timestep is 400 days (about 1/11 the orbital period of Jupiter). We work in a heliocentric coordinate system, the better to compare with the linear secular theory which uses heliocentric elements.

3.2. Results

According to the BvW theory, each set of $N_\Omega = 20$ particles having the same initial a and initial i_{free} should trace the perimeter of a single circle in p - q space at any given time, with the center of the circle yielding the local normal to the KBP. Figure 3 tests this prediction; the panels display the p - q positions of particles initially having $a = 43$ AU and $i_{\text{free}} = 0.1$ rad, sampled at four different times. Most particles at a given time do lie approximately on one circle, although there are outliers (see crosses in panels b, c, and d). The outliers represent particles whose inclinations and eccentricities grow to large values. Many of these particles suffer close encounters with Neptune, whereupon they are removed from the integration. We did not identify the cause of the instability, but probably the

various high-order mean-motion resonances in the vicinity (Nesvorný & Roig 2001) are to blame. Of the 20 particles shown at $t = 0$ in panel a, only 12 survive to $t = 4$ Gyr in panel d. Those that survive have semi-major axes that remain constant to within ± 0.5 AU.

At each t , we fit a circle (in a least squares sense) to those particles known to survive the entire length of the integration. The fit is substantially improved by also discarding particles whose instantaneous eccentricities exceed some value e_{cut} , as we find that particles on eccentric orbits tend also to be outliers in p - q space. The value of e_{cut} is reduced from one until the fit parameters cease to change significantly. Note that a particle that is discarded from the fit by the e_{cut} -criterion at one time can be restored to the fit at a later time (if its eccentricity falls below e_{cut} at that later time). Table 2 lists the values of e_{cut} chosen for the various combinations of initial a and initial i_{free} .

The circles so fitted are overlaid in Figure 3. A typical fit is excellent and the local normal of the KBP (center of the fitted circle; solid diamond) is confidently identified. Figures 4, 5, and 6 report analogous results for other choices of initial a and initial i_{free} . All 20 particles having $a = 43$ AU and $i_{\text{free}} = 0.3$ rad are stable for 4 Gyr (Figure 4). By contrast, at $a = 38$ AU, where various high-order mean-motion resonances are known to cause instability (Nesvorný & Roig 2001), only 2 out of 20 particles having $i_{\text{free}} = 0.3$ rad remain at the end of 4 Gyr (Figure 6). Fitting a unique circle to 2 points is impossible. And as is clear from Figure 6, even if we were to try fitting circles at earlier times when more particles are present, such fits would be poor. Only certain combinations of a - i_{free} permit determination of the KBP, as documented in our Table 2.

Panels d of Figures 7 and 8 plot the radii of the fitted circles versus time, for two choices of initial a - i_{free} . The BvW linear theory predicts that these radii should be constant. In fact they are nearly so, varying by at most one part out of six.

How can we further test the BvW theory when we know that it fails to predict the orbits of the planets on Gyr timescales? We compute instead a semi-analytic, BvW-based solution as follows. At each time in the numerical integration, we output the inclinations and ascending nodes of the giant planets and use these to recompute the eigenvectors—and thus the forced poles—of the linear theory. Thus we obtain a prediction of where the KBP should reside according to the linear theory at a given instant, using the simulation results for the planets at that instant to supply the integration constants. This “continuously updated BvW solution” for the local normal (forced inclination vector) is shown as an open diamond in Figures 3–6. Its location tracks that of the numerically fitted pole (solid diamond) well—much better than does the invariable pole (upright cross); see especially Figures 3 and 5. Figures 7 and 8 also demonstrate that the continuously updated BvWP hews closely to the numerically fitted KBP.

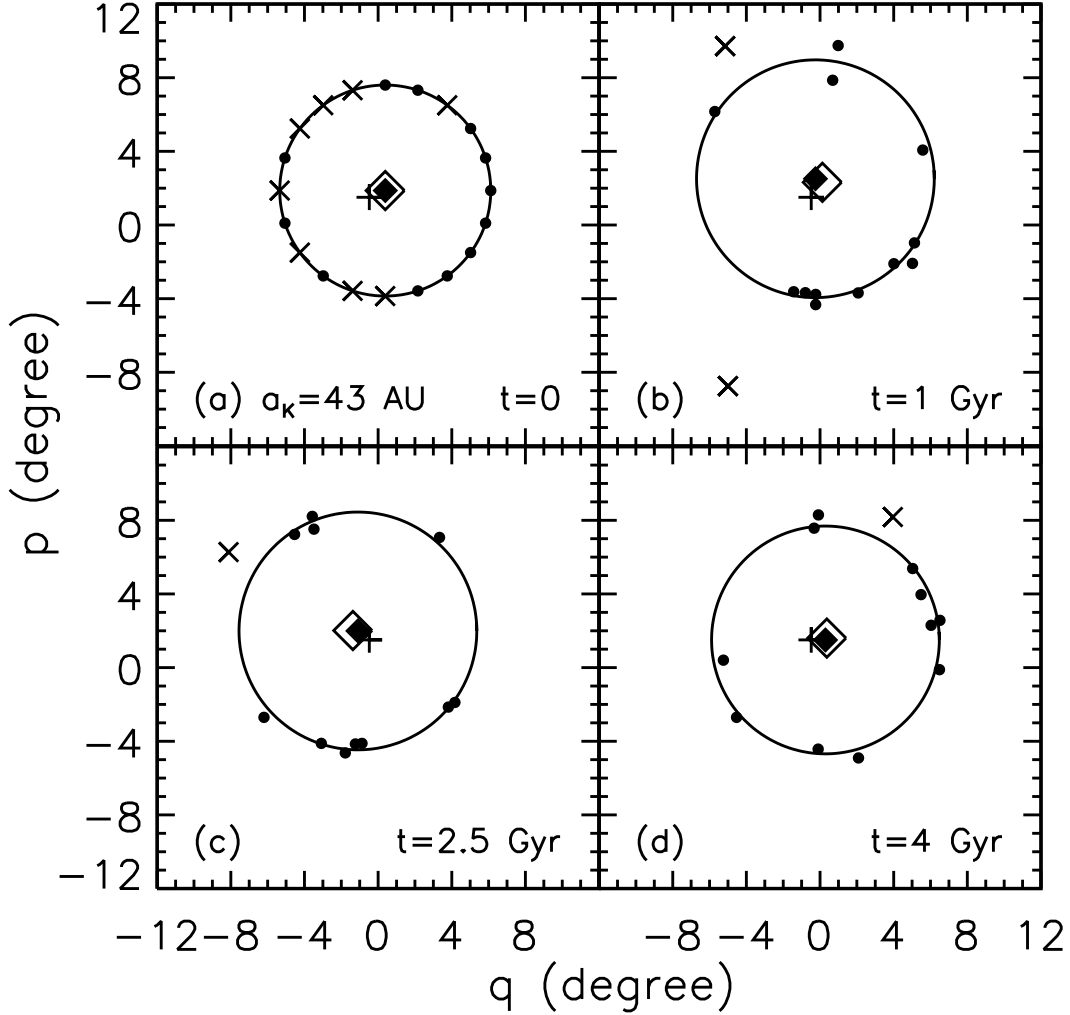


Fig. 3.— Tracking the Kuiper belt plane by numerical integration. In panel (a), we set up $N_{\Omega} = 20$ test particles having initial semi-major axes of $a_K = 43$ AU and having orbit poles distributed in a cone of half-width $i_{\text{free}} = 0.1$ rad centered on the local forced pole given by the BvW solution. In panels (b) through (d), the orbit poles evolve according to our numerical integration. Solid circles denote test particles that both survive the entire 4 Gyr duration of the integration and have osculating eccentricities less than $e_{\text{cut}} = 0.08$; these are fitted to a circle, whose center yields the local normal to the Kuiper belt plane (solid diamond). The “X” symbols denote test particles that do not satisfy these requirements. The Kuiper belt pole so obtained follows closely that predicted by the continuously updated BvW solution (open diamond), and does not point along the invariable pole (“+”).

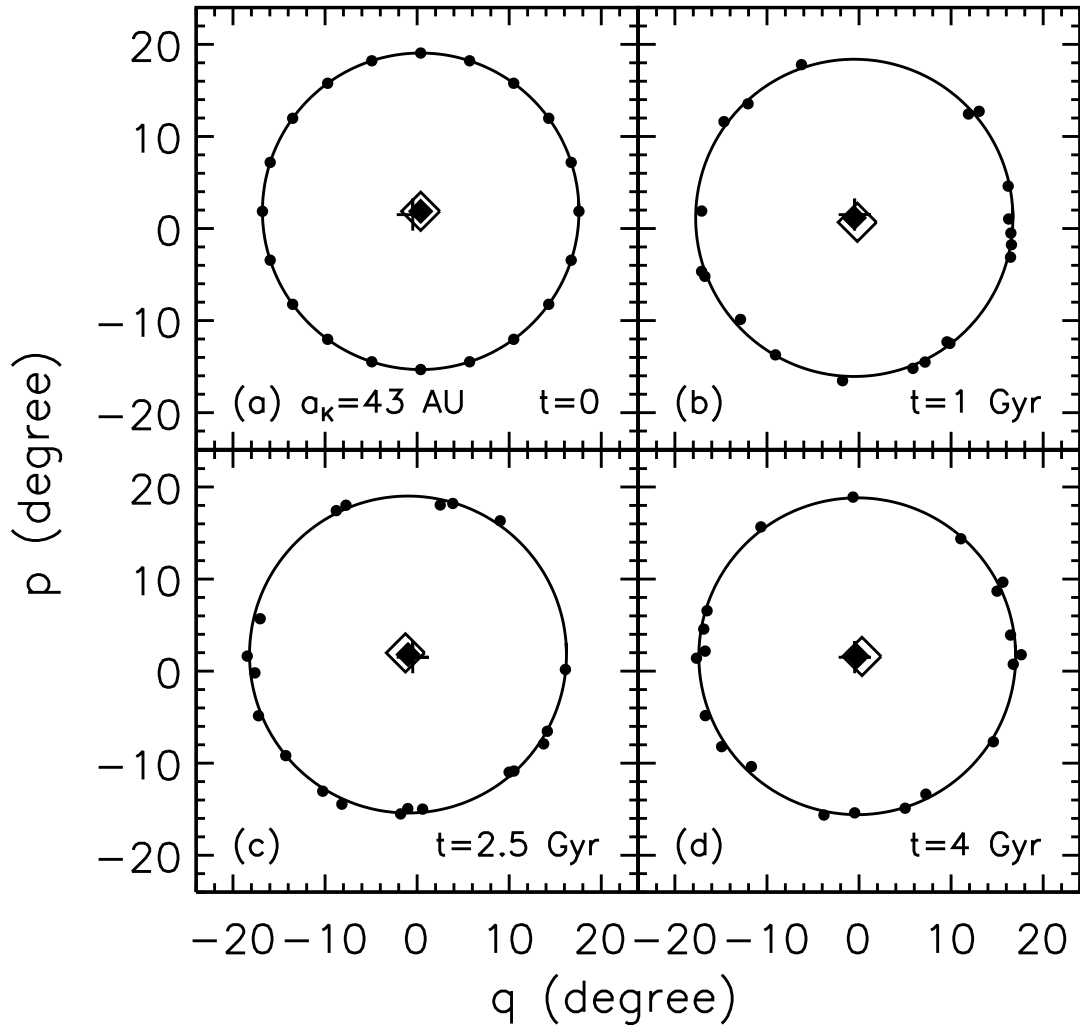


Fig. 4.— Same as Figure 3, except that initial $a_K = 43$ AU, initial $i_{\text{free}} = 0.3$ rad, and no e_{cut} criterion is applied. The numerically fitted Kuiper belt pole (solid diamond) tracks the continuously updated BvW pole (open diamond) well; both precess about the invariable pole (“+”).

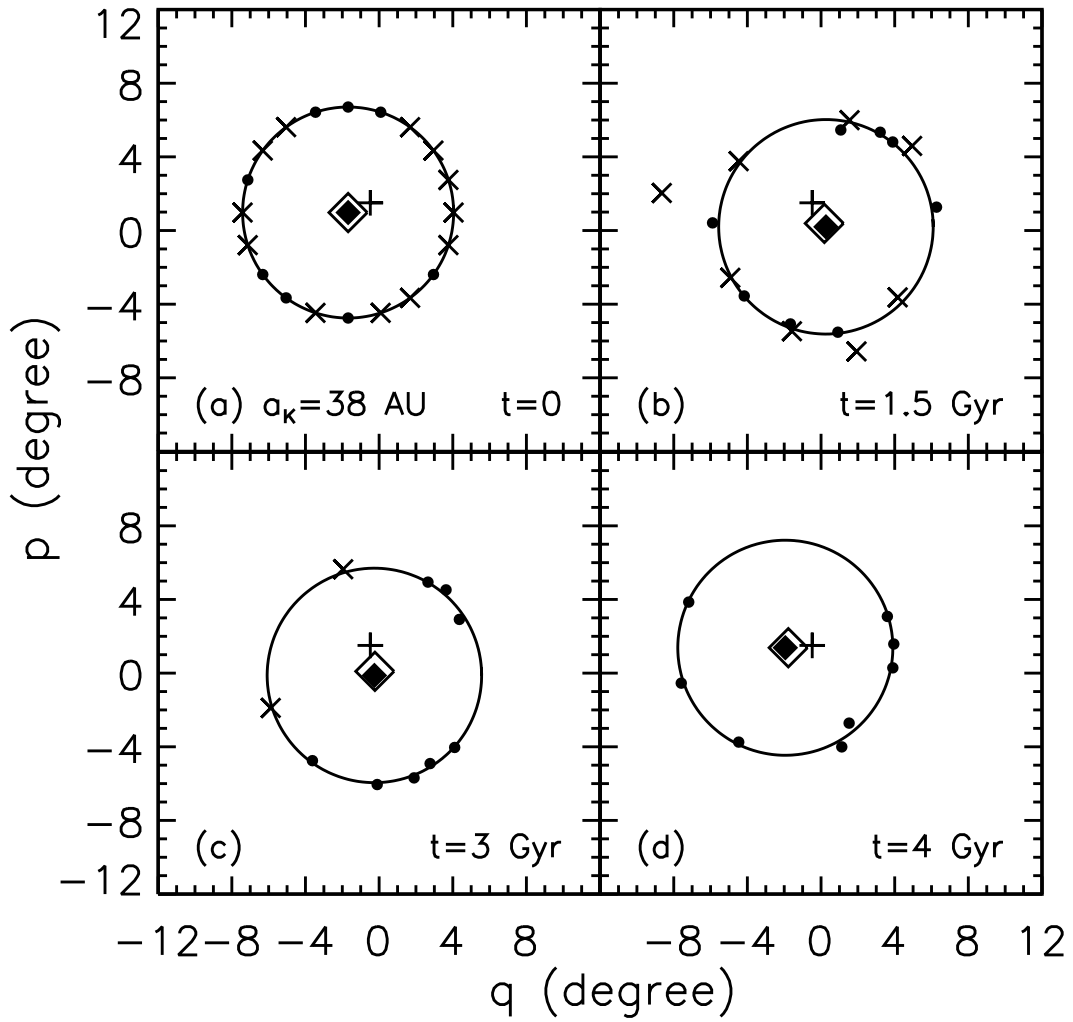


Fig. 5.— Same as Figure 3, except that initial $a_K = 38$ AU, initial $i_{\text{free}} = 0.1$ rad, and no e_{cut} criterion is applied. Here again the numerically determined Kuiper belt pole (solid diamond) is well described by the continuously updated BvW pole (open diamond), not the invariable pole (“+”).

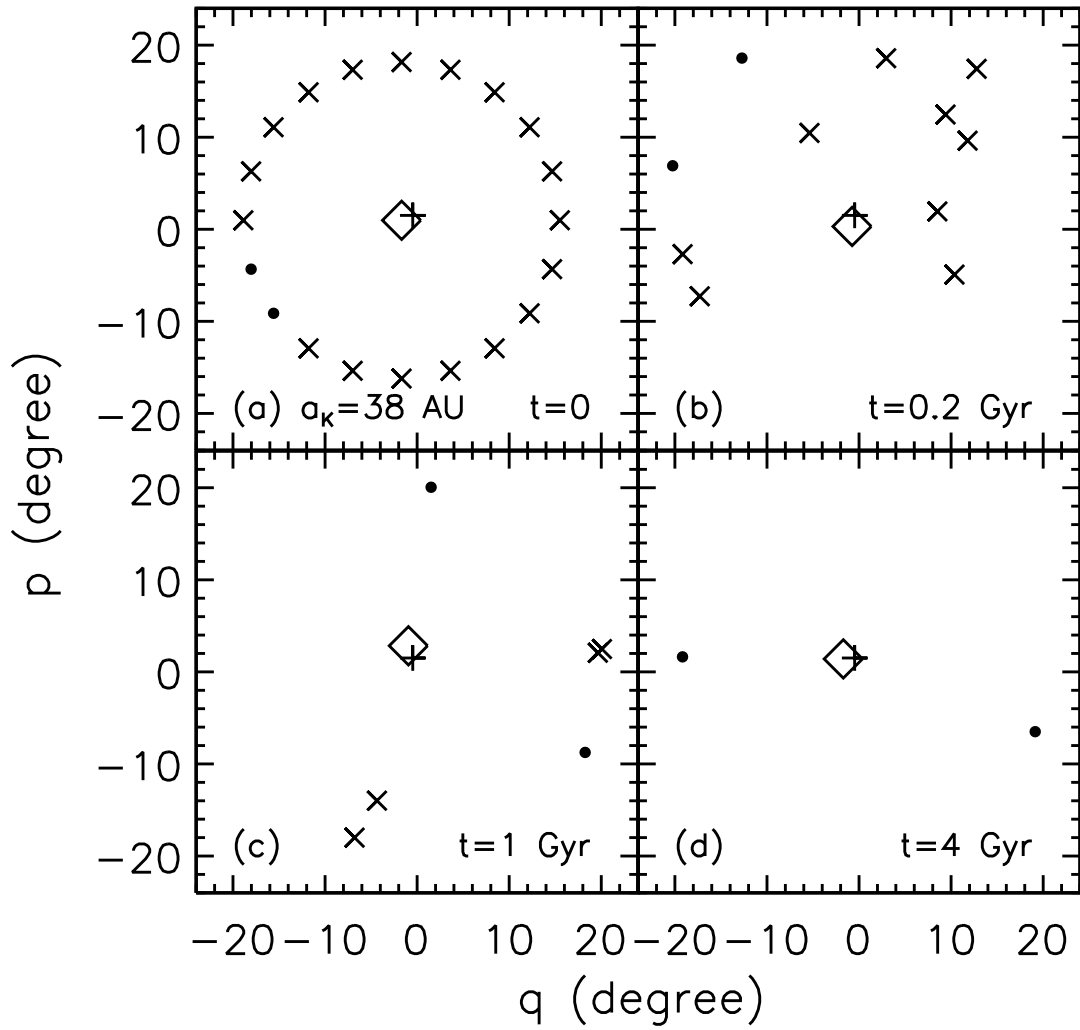


Fig. 6.— Same as Figure 3, except that initial $a_K = 38$ AU, initial $i_{\text{free}} = 0.3$ rad, and no e_{cut} criterion is applied. Only two test particles survive the 4 Gyr duration of the integration, rendering determination of the Kuiper belt pole impossible.

To summarize the results of our numerical simulations: Linear secular theories like BvW correctly predict how the warped KBP evolves with time, provided the parameters of those analytic theories are continuously updated using either observations or numerical simulations of the giant planets’ orbits. The KBP today is accurately predicted by the updated BvW solution. The KBP does not, in general, coincide with the invariable plane, except at infinite distance from the planets.

4. THEORY VERSUS OBSERVATION

We have shown by numerical simulations in §3 that the Classical KBP is given by the BvWP, i.e., by linear secular theory. Here we assess whether observations of KBOs bear out this result, by locating the actual poles of the KBP near 38 AU and 43 AU. These semi-major axes lie to either side of the ν_{18} resonance; theory predicts that the corresponding poles should lie to either side of the invariable pole, with all three orbit normals lying in one plane (see Figure 1). Our dataset consists of KBOs listed on the Minor Planet Center website on Jan 22 2008 whose (a) astrometric arcs extend longer than 50 days (many objects in our sample have much longer arcs), (b) eccentricities are less than 0.1, (c) inclinations are less than 10 degrees, and (d) are classified by the Deep Ecliptic Survey (DES) as “Classical” in at least two out of their three orbital integrations (see Elliot et al. 2005 for a description of the classification scheme). In the vast majority of cases, all three DES integrations yield a classification of “Classical.” Moreover, the typical 3σ uncertainties in semi-major axes are smaller than ~ 0.1 AU. We assemble two samples, one for which $38.09 \text{ AU} < a < 39.10 \text{ AU}$ (the “38 AU” sample, containing 10 objects) and another for which $42.49 \text{ AU} < a < 43.50 \text{ AU}$ (the “43 AU” sample, containing 80 objects). Object designations are given in Table 3.

Figure 9 plots the observed (q,p) positions for the two samples, and compares with theory. Theory predicts that the average (\bar{q}, \bar{p}) measured for each sample should equal $(q_{\text{forced}}, p_{\text{forced}})$ calculated for the average semi-major axis of the sample. The good news is that the data are consistent with this prediction; the differences between the observed poles and the forced poles are less than 2σ for both samples (the error bars in Figure 9 are $\pm 3\sigma$, where σ is the standard deviation of the mean). The bad news is that the observed poles are also consistent with the invariable pole, at a similar confidence level. While it is encouraging for the theory that the observed pole at 38 AU indeed lies to the left (toward smaller q) of the invariable pole, and that the observed pole at 43 AU lies to the right, there are not enough observations to make more precise statements and to rule out the hypothesis that the KBP equals the IP with greater than 3σ confidence.

Note that by selecting our sample to have orbital inclinations less than 10 degrees with

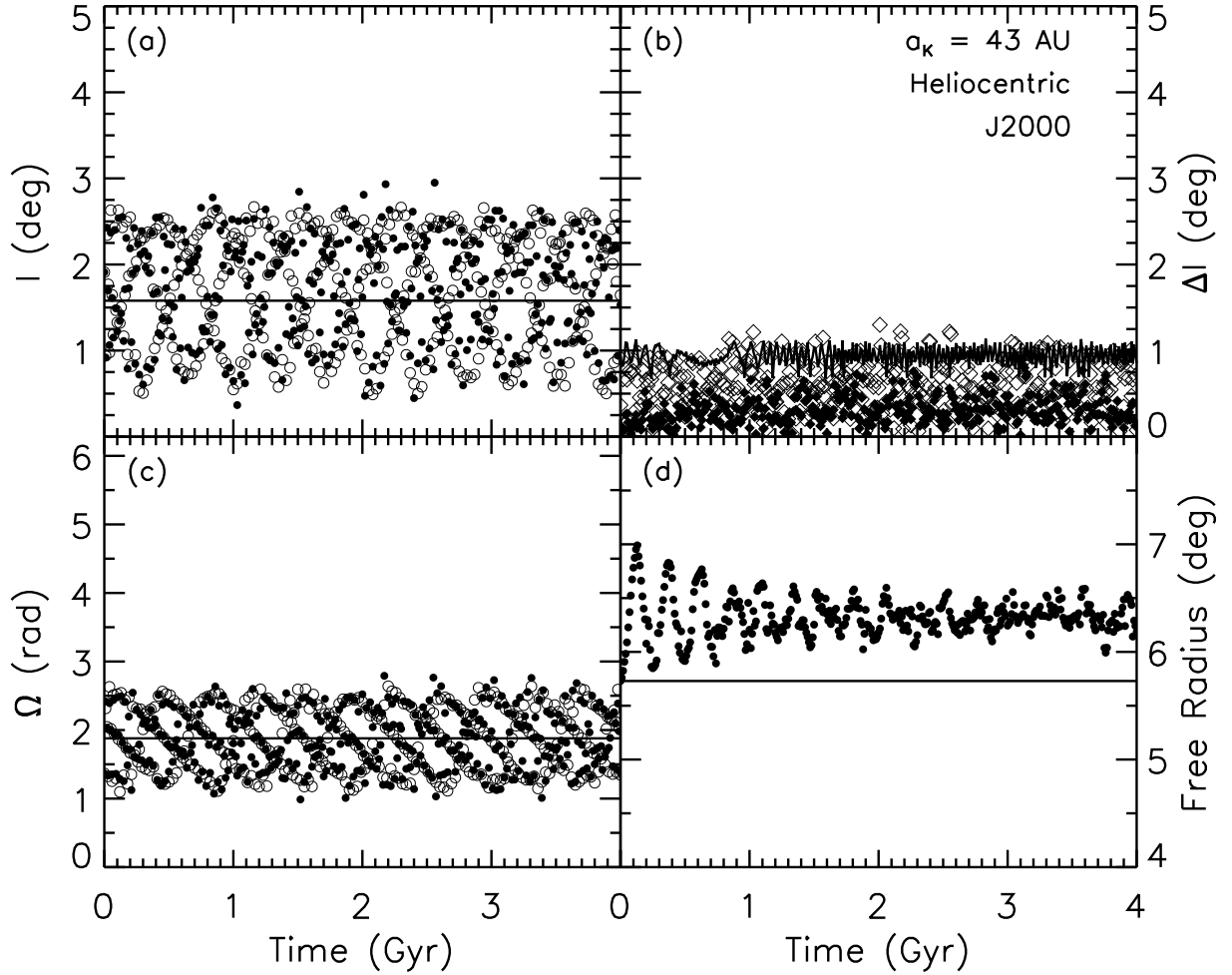


Fig. 7.— Results for test particles having initial $a_K = 43 \text{ AU}$ and initial $i_{\text{free}} = 0.1 \text{ rad}$, demonstrating that the numerically obtained KBP follows the continuously updated BvWP, not the IP. (a) Inclination of the KBP (solid circles), BvWP (open circles), and IP (line), all relative to the ecliptic. (b) Mutual inclination between the KBP and BvWP (solid diamonds), the BvWP and the IP (open diamonds), and the KBP and the IP (solid line). (c) Longitude of ascending node of the KBP (solid circles), BvWP (open circles), and IP (line), all relative to the ecliptic and mean equinox of J2000. (d) Numerically obtained free inclination (solid circles; these are the radii of the fitted circles in Figure 3), compared against the initial i_{free} (line). The BvW theory predicts that the free inclination should be constant; while it is nearly so in our numerical integration, its mean value is offset by 0.6 deg (10%) relative to its initial value. Data are sampled every 10^8 yr and do not resolve the precession of the KBP occurring with a $\sim 10^6\text{-yr}$ period (see Figure 10).

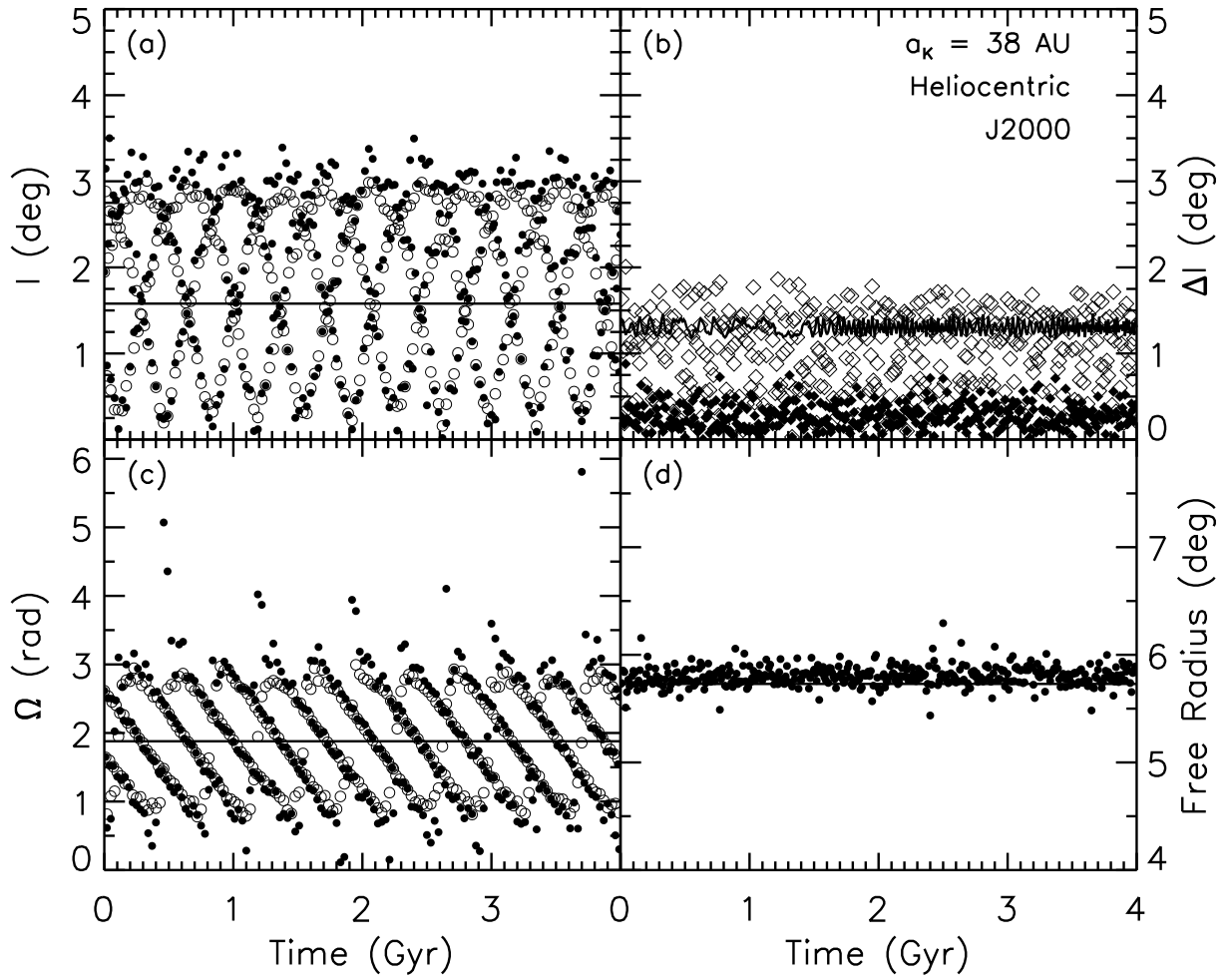


Fig. 8.— Same as Figure 7, except for initial $a_K = 38$ AU and initial $i_{\text{free}} = 0.1$ rad.

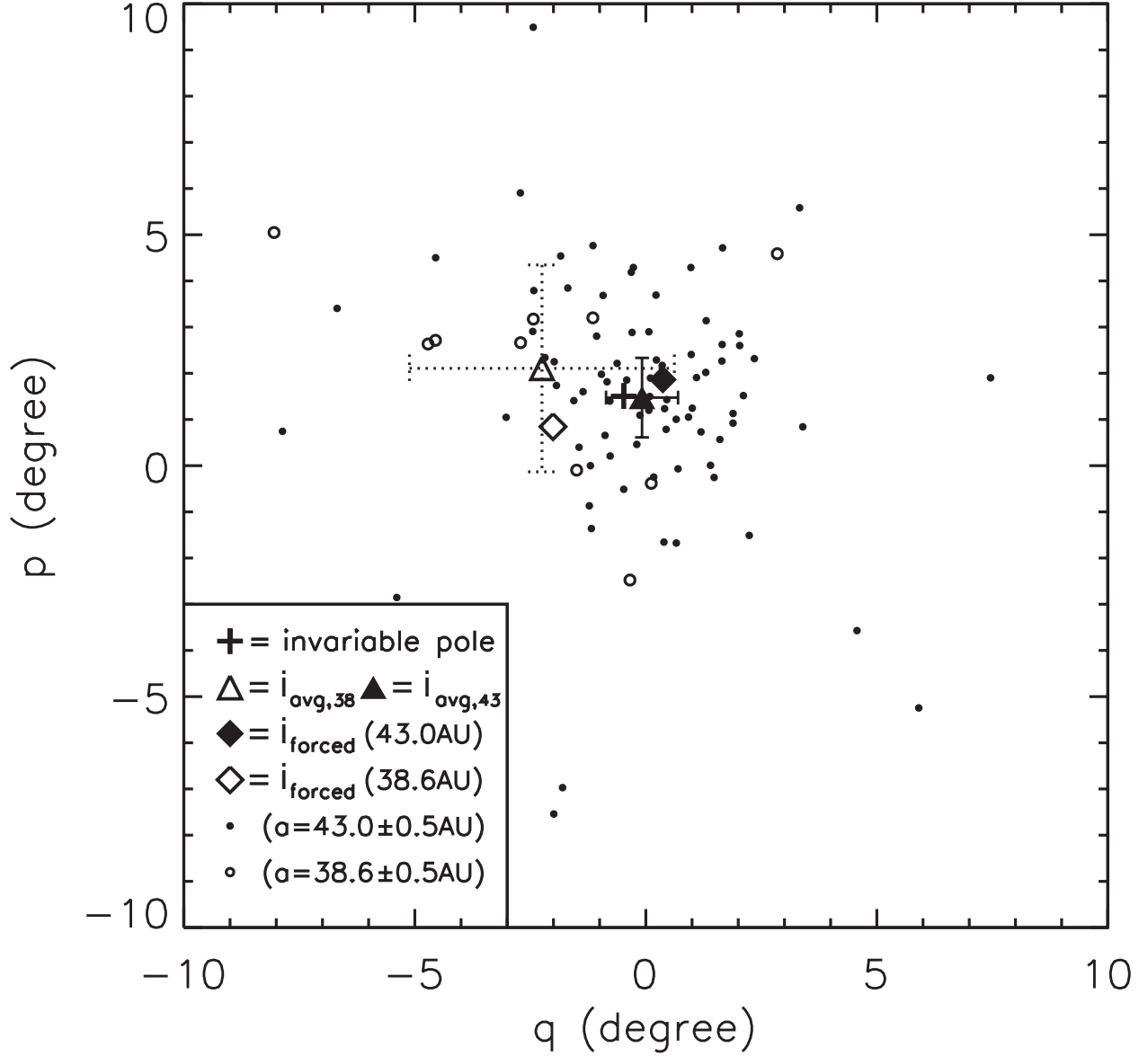


Fig. 9.— Pole positions of observed Classical KBOs having semi-major axes near 38 AU (open circles) and 43 AU (filled circles), in $q = i \cos \Omega, p = i \sin \Omega$ space, referenced to the J2000 ecliptic. According to theory (§2–§3), the average pole position at a given semi-major axis (triangles with error bars) should match the forced pole positions (diamonds) calculated from BvW. They do to within 2σ (error bars are $\pm 3\sigma$, where σ is the standard deviation of the mean). Unfortunately, the alternate hypothesis that the average pole positions are given by the invariable pole (bold cross) cannot be ruled out with greater confidence.

respect to the ecliptic plane, we bias our measurement of the average pole position towards the ecliptic pole. This systematic error is probably still smaller, however, than our random error. For example, the observed pole at 38 AU actually lies further from the ecliptic pole than does the theoretically expected forced pole. See Elliot et al. (2005) for ways of reducing this systematic bias.

We also performed a two-dimensional Kolmogorov-Smirnov test to see whether the (q, p) distributions for the two samples differ (they should). The probability that they do not is 4.9%—small enough to be suggestive of a real difference, but in our judgement too large to be conclusive.

5. SUMMARY AND DISCUSSION

Classical Kuiper belt objects trace a sheet that warps and precesses in response to the planets. The current location and shape of this sheet—the “plane” of the Classical Kuiper belt—can be computed using linear secular theory, with the observed masses and current orbits of the planets as input parameters (Brown & Pan 2004). The local normal to the plane is given by the theory’s forced inclination vector, which is specific to every semi-major axis. At infinite distance from the planets, the plane coincides with the invariable plane. The deviations of the Kuiper belt plane away from the invariable plane, while generally non-zero, are typically small: less than 3 degrees outside the secularly unstable gap at $a \approx 40.5 \pm 1$ AU (inside the gap no KBOs have been observed, as expected). As the semi-major axis varies from < 40.5 AU to > 40.5 AU, the ascending node of the Kuiper belt plane on the invariable plane rotates by very nearly 180 degrees, a result of the sign change in the forced response across the ν_{18} resonance.

These conclusions are supported by our numerical integrations of giant planet and test particle orbits lasting 4 Gyr. These integrations show that a Kuiper belt object maintains a nearly fixed orbital inclination with respect to the time-variable Kuiper belt plane. This accords with linear theory, in which the free inclination represents the undamped, constant amplitude of a test particle’s free oscillation. It may seem surprising that the linear theory is vindicated in this regard while it cannot accurately predict planetary motions and hence the future location of the Kuiper belt plane. But the inaccuracies accrue only slowly—Figure 10 shows that it takes several precession periods for the linear theory to diverge from numerical simulation in predicting the location of the plane, and the analytic and numerical solutions are always qualitatively similar. Referring back to the equations of motion (5)–(6), we see that if we take the planetary forcing terms $q_j(t)$ and $p_j(t)$ to be given by the more realistic numerical integration—instead of the inaccurate but qualitatively similar analytic

solution (3)–(4)—then the free component of the motion (the homogeneous solution of the differential equation) would still be given by (7)–(8), irrespective of the forced component (the inhomogeneous solution). Thus an object can keep its free inclination with respect to the forced plane fixed, even though the location of the forced plane itself cannot be forecast analytically.

Currently the data on actual KBOs are consistent with, but do not conclusively verify, our theoretical finding that the Kuiper belt plane warps by a few degrees to either side of the secularly unstable gap. Our analysis of the observations, like that of Elliot et al. (2005), suffers from large random errors. The study by Brown & Pan (2004) does not, but at the expense of including objects of all dynamical classes and not following variations in the pole position with semi-major axis. Quadrupling the sample size of low- i , low- e objects at 38 AU, where there are currently ten usable objects, can increase our confidence in the reality of the warp to greater than 3σ .

Detecting “Planet X” via its influence on the Kuiper belt plane will be substantially more challenging. We calculate that a $100-M_{\oplus}$ planet with a semi-major axis of 300 AU and an orbital inclination with respect to the ecliptic of 10 degrees would shift the forced poles in the 43–50 AU region by 0.1 degree.

We thank Ruth Murray-Clay and Mike Brown for discussions, and Chris Culter for suggesting this undergraduate research collaboration. An anonymous referee provided numerous helpful comments. This work was supported by NSF grant AST-0507805.

REFERENCES

- Brouwer, D., & van Woerkom, A.J.J. 1950, The Secular Variations of the Orbital Elements of the Principal Planets (Astron. Pap. Am. Ephemeris Naut. Alm., 13, 81) (Washington: GPO)
- Brown, M.E., & Pan, M. 2004, *AJ*, 127, 2418
- Chiang, E., et al. 2007, in *Protostars and Planets V*, ed. B. Reipurth, D. Jewitt, & K. Keil (Tucson: University of Arizona Press)
- Elliot, J.L., et al. 2005, *AJ*, 129, 1117
- Gaudi, B.S., & Bloom, J.S. 2005, *ApJ*, 635, 711
- Levison, H.F., & Duncan, M.J. 1994, *Icarus*, 108, 18

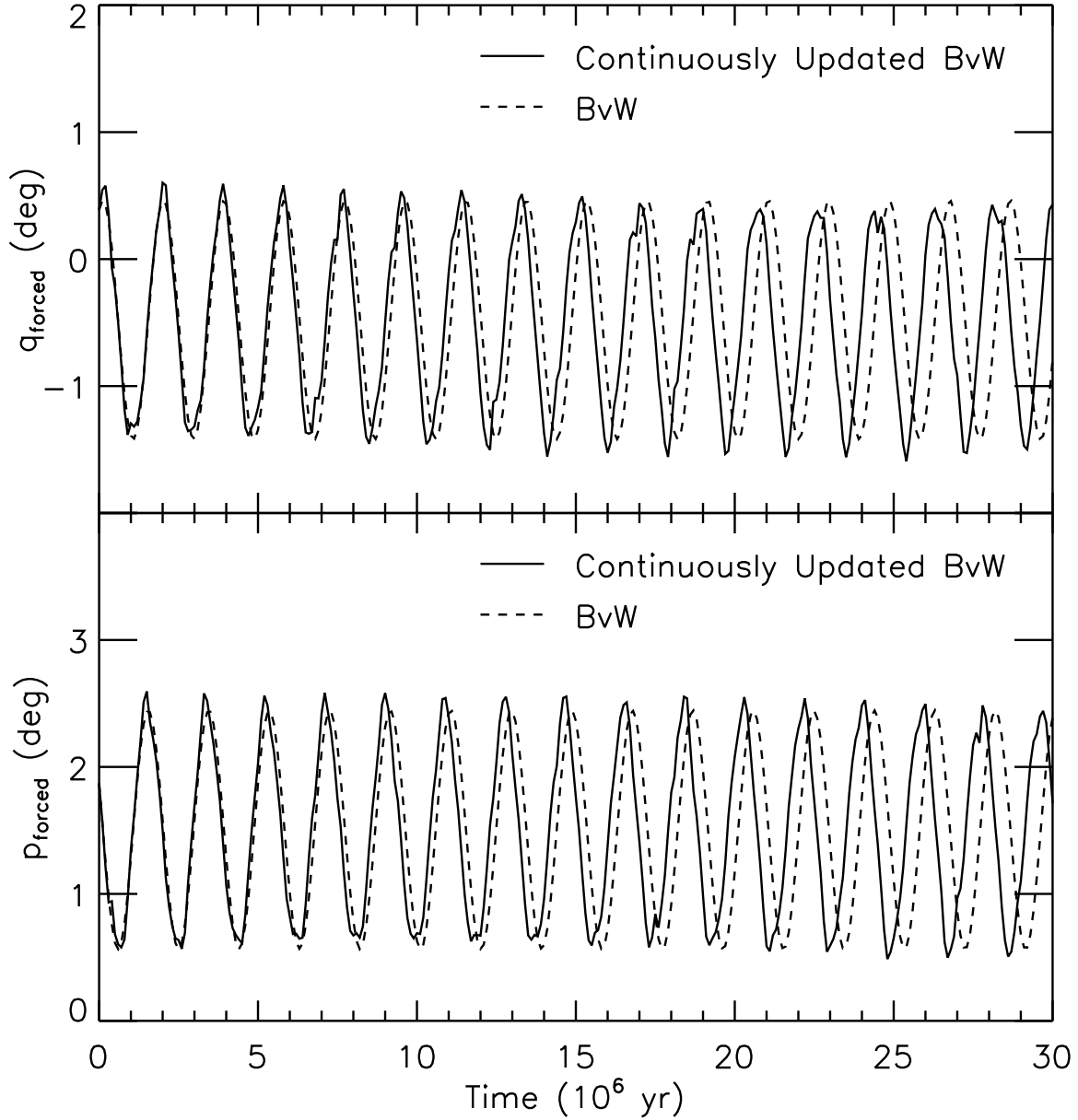


Fig. 10.— Components of the forced pole versus time, computed using the BvW theory (dashed line) and the continuously updated BvW theory (solid line). The latter uses the results of numerical integrations at every timestep to reset its parameters, and is therefore essentially a numerical solution. While the numerical solution eventually diverges from the BvW solution, the two are qualitatively similar.

Murray, C.D., & Dermott, S.F. 1999, *Solar System Dynamics* (Cambridge: Cambridge University Press)

Nesvorný, D., & Roig, F. 2001, *Icarus*, 150, 104

Wisdom, J., & Holman, M. 1991, *AJ*, 102, 1528

Table 1. BvW solution^a for Jan 1, 2000 ($t = 0$)

	$k = 1$	2	3	4
$j = 1$	1.5792	0.36081	0.055195	-0.066653
2	1.5792	-0.89904	0.044853	-0.064203
3	1.5792	0.040670	-1.01200	0.062630
4	1.5792	0.0045122	0.11941	0.67290
f_k	0	-123.13	-14.102	-3.2984
γ_k	1.8788	-0.91730	2.3699	-2.7418

^aThe components I_{jk} of the eigenvectors (in degrees), eigenfrequencies f_k (in radians per Myr), and phases γ_k (in radians), calculated using data for the giant planets on JD = 2451544.5 from NASA JPL Horizons. All elements are heliocentric and referred to the ecliptic and mean equinox of J2000.

Table 2. Numerical Results for Stability in Initial a - i_{free} Space

a (AU)	i_{free} (rad)	# of Survivors (out of 20)	e_{max} of Survivors	e_{cut}	Permits KBP Determination?
38	0.01	17	0.05	None Applied	Yes
	0.03	16	0.05	None Applied	Yes
	0.10	8	0.07	None Applied	Yes
	0.30	2	0.02	None Applied	No
43	0.01	19	0.12	0.04	Yes
	0.03	20	0.04	None Applied	Yes
	0.10	12	0.12	0.08	Yes
	0.30	20	0.02	None Applied	Yes
44	0.01	20	0.11	0.03	Yes
	0.03	20	0.11	0.04	Yes
	0.10	20	0.15	0.06	Yes
	0.30	20	0.29	0.08	Yes

Table 3. Samples of Observed KBOs for Locating the KBP

Sample	Objects
“38 AU”	1998 WV ₂₄ , 1999 OJ ₄ , 2000 YB ₂ , 82157, 2003 FD ₁₂₈ , 2003 QA ₉₂ , 2003 YL ₁₇₉ , 2003 QQ ₉₁ , 144897, 119951
“43 AU”	19255, 1994 EV ₃ , 1996 TK ₆₆ , 33001, 1998 WY ₂₄ , 1998 WX ₂₄ , 1999 CN ₁₅₃ , 1999 RT ₂₁₄ , 1999 ON ₄ , 1999 XY ₁₄₃ , 1999 RW ₂₁₄ , 1999 CH ₁₅₄ , 1999 RU ₂₁₅ , 1999 HV ₁₁ , 1999 DA, 1999 HJ ₁₂ , 1999 CW ₁₃₁ , 2000 PU ₂₉ , 2000 PX ₂₉ , 134860, 2000 CL ₁₀₅ , 2000 ON ₆₇ , 2000 PC ₃₀ , 2000 FS ₅₃ , 2000 WV ₁₂ , 2000 WL ₁₈₃ , 2000 OU ₆₉ , 2000 YU ₁ , 88268, 2001 QB ₂₉₈ , 2001 QD ₂₉₈ , 2001 XR ₂₅₄ , 2001 QO ₂₉₇ , 2001 HZ ₅₈ , 2001 RW ₁₄₃ , 2001 OK ₁₀₈ , 2001 DB ₁₀₆ , 88267, 2001 XU ₂₅₄ , 2001 FK ₁₈₅ , 2001 OZ ₁₀₈ , 2002 CD ₂₅₁ , 2002 PX ₁₇₀ , 2002 PV ₁₇₀ , 2002 FW ₃₆ , 2002 WL ₂₁ , 160256, 2002 VB ₁₃₁ , 2002 PY ₁₇₀ , 2002 CS ₁₅₄ , 2002 PD ₁₅₅ , 2003 SN ₃₁₇ , 2003 UT ₂₉₁ , 2003 FK ₁₂₇ , 2003 QG ₉₁ , 2003 FA ₁₃₀ , 2003 HY ₅₆ , 2003 QY ₉₀ , 2003 TK ₅₈ , 2003 QF ₉₁ , 2003 QE ₉₁ , 2003 QZ ₁₁₁ , 2003 QL ₉₁ , 2003 QE ₁₁₂ , 2003 YR ₁₇₉ , 2003 QY ₁₁₁ , 2003 QD ₉₁ , 2003 TL ₅₈ , 2003 QU ₉₀ , 2003 YT ₁₇₉ , 2003 YX ₁₇₉ , 2003 YS ₁₇₉ , 2003 YJ ₁₇₉ , 2004 UD ₁₀ , 2004 DM ₇₁ , 2005 JZ ₁₇₄ , 2005 GD ₁₈₇ , 2005 JP ₁₇₉ , 2005 XU ₁₀₀ , 2006 HA ₁₂₃